ELSEVIER

Contents lists available at ScienceDirect

Journal of Magnetism and Magnetic Materials

journal homepage: www.elsevier.com/locate/jmmm



Research articles

Alignment of collagen matrices using magnetic nanowires and magnetic barcode readout using first order reversal curves (FORC) (invited)



Anirudh Sharma ^a, Michael D. DiVito ^b, Daniel E. Shore ^c, Andrew D. Block ^a, Katie Pollock ^b, Peter Solheid ^d, Joshua M. Feinberg ^d, Jaime Modiano ^e, Cornelius H. Lam ^f, Allison Hubel ^{b,f}, Bethanie J.H. Stadler ^{a,c,*}

- ^a Department of Electrical and Computer Engineering, University of Minnesota, Minneapolis, MN 55455, United States
- ^b Department of Mechanical Engineering, University of Minnesota, Minneapolis, MN 55455, United States
- ^c Department of Chemical Engineering and Materials Science, University of Minnesota, Minneapolis, MN 55455, United States
- ^d Department of Earth Sciences and Institute of Rock Magnetism, University of Minnesota, Minneapolis, MN 55455, United States
- ^e Veterinary Clinical Services and Masonic Cancer Center, University of Minnesota, Minneapolis, MN 55455, United States
- f Department of Neurosurgery, University of Minnesota, Minneapolis, MN 55455, United States

ARTICLE INFO

Article history: Received 11 July 2017 Received in revised form 29 October 2017 Accepted 8 November 2017 Available online 9 November 2017

Keywords:
Collagen
Magnetic alignment
Blood-brain-barrier
Arachnoid cells
Osteosarcoma
Magnetic nanowires
FORC
Nano barcodes

ABSTRACT

Collagen matrices are one form of artificial tissue that has applications in biomimetic organs or tumors, and in fundamental biology. Anatomical organs and tissues are often composed of aligned collagen, and in this study cross-linking nickel magnetic nanowires (MNWs) to collagen allowed a one-step bidirectional alignment of the collagen matrices when processed in a uniform magnetic field. These matrices were analyzed by differential interference contrast (DIC) microscopy, scanning electron microscopy (SEM) and polarized transmittance. The bi-directional alignment was also confirmed by plated, stained arachnoid cells from the blood-brain-barrier (BBB). Arachnoid cells are morphologically sensitive to their extracellular matrix (ECM) environment, and in this study, they were observed to spider out in two distinct directions as predicted by microscopy and transmittance. In fact, MNW-collagen matrices plated with arachnoid-cells are promising for future studies of artificial BBBs. Other cells (here osteosarcoma) have been observed to internalize MNWs, which leads to the possibility of barcoding matrices and cells with distinct signatures, pending a magnetic readout technique. To this aim, mixtures of two different MNW populations were analyzed using first order reversal curves (FORC), and the relative concentrations of the two populations were correctly estimated with negligible error for ratios of 1: 23 and only 7% error for ratios of 1: 115. Together, these studies open a path for magnetic identification of artificial tissues where distinct magnetic labels on matrices and in cells combine for a unique fingerprint.

© 2017 Published by Elsevier B.V.

1. Introduction

Simultaneous, multiplexed diagnoses using large bioassays or tissue biopsies is possible via magnetic techniques, and much effort has been invested in tuning the magnetic properties of magnetic nanoparticles (MNPs) [1–4]. However, MNPs are recently almost exclusively used for separation (aka enrichment) with multiplexed diagnoses occurring by means other than magnetic signatures, for example by mass spectroscopy [5], photoacoustics [6], nuclear magnetic resonance [7], flow [8], or by moment (measuring the number of MNPs, not the type of MNP). This research has largely been driven by a narrowing focus on the detection of sparse

E-mail address: stadler@umn.edu (B.J.H. Stadler).

analytes. Indeed, zeptomolar detection limits (10^{-16}) have been achieved [9,10], which could be important in early detection of diseases, such as cancer.

However, there are medical applications for multiplexing that do not require zeptomolar detection. One example is immunotherapy in cancer, where many leukocytes may reach a tumor site, and the important parameter under study is the ratio of cell types present. In these cases, ratios as low as 1:10 are of interest, and the total number of detected cells is not small. Another example is labeling, or 'barcoding,' artificial tissue such that the source of the tissue can be identified at a later date by tissue manufacturers, researchers, or medical personnel.

Here, magnetic nanowires (MNWs) were used in the processing of collagen matrices for two reasons. First, MNWs in a tissue matrix can contribute part of the magnetic barcode for the sample. Second, it was hypothesized that low magnetic fields could be used

^{*} Corresponding author at: Department of Electrical and Computer Engineering, University of Minnesota, Minneapolis, MN 55455, United States.

to align the collagen fibrils, a feat otherwise accomplished by compressive strain [11–13], electrospinning [14,15]; shear force [16]; or very high magnetic fields [17]. MNWs have a unique shape anisotropy that can be aligned by an external field to produce matrix alignment either indirectly by steric effects or by directly crosslinking MNWs to the collagen. Surprisingly, a bi-directional alignment of the collagen fibers was achieved when cross-linking was used, which leads to improved mechanical properties compared to the unidirectional alignment produced by other methods. In fact, naturally occurring collagen in many tissues, such as bone and cornea, exhibit bidirectional arrangements of fibrils [18].

To help visualize the 3D structure of the bi-directional alignment, and to mimic an important biological tissue, arachnoid cells were embedded into the gels. In vivo, arachnoid cells occupy the border between the central nervous system's liquid milieu and the vascular system on one side of the blood brain barrier [19,20]. The extracellular matrix inhabited by these cells reflects a variety of architectures, from thin sheets to complex threedimensional structures abutting the blood. The morphology of arachnoid cells is influenced by the architecture of the extracellular matrix resulting in a spider-like shape for the cells (hence the name). Therefore, fluorophore-stained arachnoid cells were used here to visualize the 3D architecture of our matrices. Osteosarcoma cells were also incubated directly with Ni MNWs labeled with RGD, a peptide that binds to integrin which is overexpressed by osteosarcoma. The MNWs were internalized by the osteosarcoma, revealing the possibility to label matrices and cells with distinct barcodes if the right combination of MNW labels and magnetic 'readout' can be found.

For this reason, a new approach is introduced here for magnetic readout. Major magnetic hysteresis loops (ie: applied fields swept from positive to negative saturation) are sufficient for determining the structure of most thin film samples, like spin valves, typically by observing coercivities. For MNWs, however, sheared hysteresis loops can occur due to factors such as interwire interactions, intersegment interactions (in segmented MNWs), and switching field distributions. This shearing makes it difficult to distinguish different values of coercivity in mixtures. Therefore, first order reversal

curves (FORC) were used here to derive coercivity distributions for MNWs that have varying interaction fields, and then several MNW mixtures were de-multiplexed using FORC.

2. Materials and methods

Nickel (Ni) MNWs were made by electrochemical deposition inside nanoporous anodic aluminum oxide templates using previously established methods [21]. To functionalize their surface with amine groups, the MNWs were rinsed with DI water and suspended in an NH2-PEG-COOH solution (0.2 mass%, pH 7) at concentrations in the range of 10–100 million MNW/ml. The samples were sonicated for 10 min and stored at 4 °C overnight. The PEG solution was decanted from the MNWs, and replaced with 0, 0.002 or 0.2 M CDI solution (0.1 mM HCl, pH 3). The samples were sonicated for 10 min and stored at room temperature overnight. The CDI was then decanted, and the MNWs were rinsed with 1 mM HCl. The basic schematic of cross-linking collagen fibrils to magnetic MNW surfaces is shown in Fig. 1(a).

The MNWs were suspended in a type I collagen solution (5 mg/ml, pH 3) at concentrations of 0.1, 1, and 10 million MNW/ml and stored overnight. After 12 h, the MNW-collagen solution was placed in the center of a uniform magnetic field (0.1 T) for 2 min to allow for MNW alignment. The collagen solution was neutralized by exposure to ammonia vapor. For optical imaging, the MNW-collagen matrices were fixed in a 3.7% formaldehyde-DPBS solution. For electron imaging, the matrices were fixed in a 2% glutaraldehyde solution containing 0.1 M sucrose and 0.1 M sodium cacodylate for 1 h at room temperature. These samples were then post-fixed in a 1% osmium tetroxide solution for 30 min, after which they were soaked in ethanol solutions with slowly increasing concentrations before critical-point drying and Pt coating. Images using secondary electron microscopy were obtained using a 5 kV beam.

Immortalized arachnoid cells, isolated from rat arachnoid meninges using previously described procedures [22], were seeded on the MNW-collagen matrices at densities of 16,000 cells/cm².

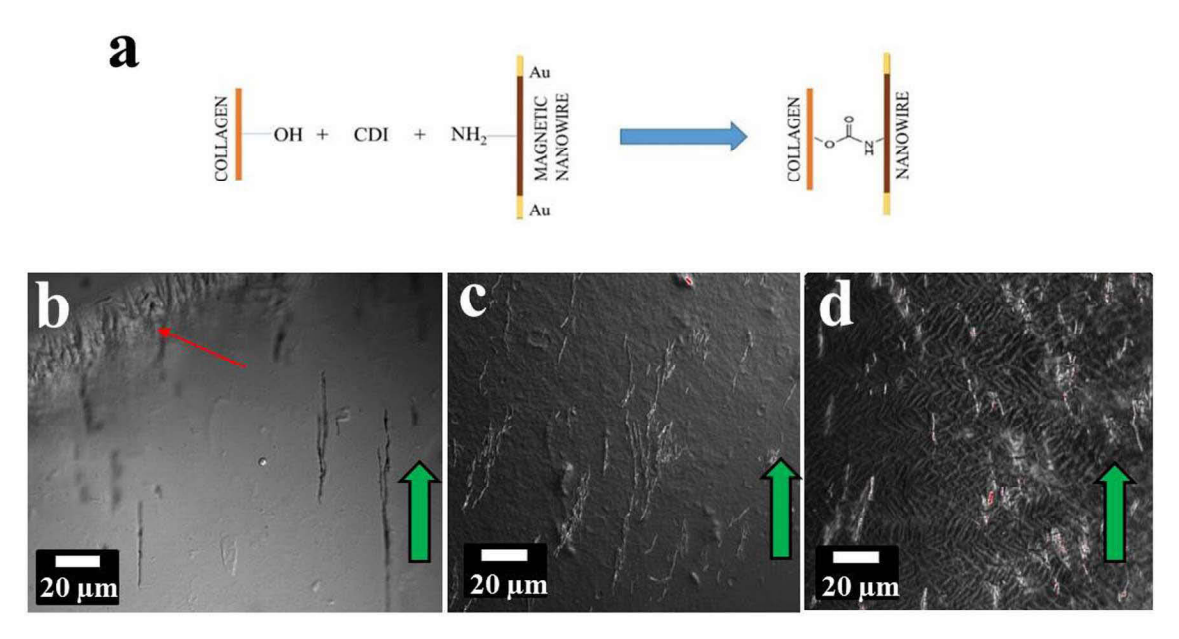


Fig. 1. a) Schematic of cross-linking chemistry between collagen and Ni MNWs. (b-d) DIC cross section images of MNW-collagen matrices (Ni MNWs:160 nm diameter, 6 μm length) neutralized in a magnetic field applied in the direction shown by green arrows. (b) Matrix containing 0.2 M CDI and 1 million MNW/ml. An apparent corrugation was observed only at the edges (red arrow) where meniscus effects lead to increased local MNW concentration. (c) Matrix containing 0.02 M CDI and 10 million MNW/ml. Bi-directional corrugation was observed throughout this last sample, suggesting bi-directional collagen alignment.

After 72 h, cells were fixed, stained and imaged. For future artificial tumor studies, osteosarcoma cells were also labeled with MNWs according to previously described protocols [23]. Osteosarcoma cells were chosen because the cells express a high density of membrane integrins [24–26], thus ensuring uptake via RGD-labeling of MNWs, which subsequently enable unique magnetic tissue identification.

In first order reversal curve (FORC) analysis [27], a sample is saturated at a high positive field, then the field (H) is reduced to a reversal field (H_r) and the moment is measured as the field is swept back to positive saturation. A family of curves is measured using successively more negative reversal fields, and the double derivative

$$\rho(H, H_r) = -\frac{1}{2} \frac{\delta^2 M}{\delta H_r \delta H} \tag{1}$$

is plotted vs two axes that indicate interaction field ($H_{\rm u}$) and coercivity ($H_{\rm c}$), defined by

$$H_u = \frac{H + H_r}{2}$$
 and $H_c = \frac{H - H_r}{2}$ (2)

3. Results

3.1. Bi-directionally oriented collagen matrices

The first part of this work dealt with the potential of MNWs in collagen matrices to magnetically align the collagen fibrils and to provide a means of identification via magnetic readout. Collagen solutions were prepared with varying ratios of 100 nm-diameter Ni MNWs (0.1, 1, 10 million MNW/ml) and CDI cross-linker (0, 0.002, 0.2 M) before fixation in the presence of a uniform magnetic field. Differential interference contrast (DIC) microscopy was used in conjunction with two cross-polarizers to image the resulting matrix, Fig. 1. The matrices appeared unaffected by MNWs except at the higher concentrations of both MNWs and CDI. A corrugated pattern emerged at 10million MNW/ml and 0.2 M CDI that was only otherwise observed at the edges of samples with fewer MNWs but the same CDI. In the latter matrices, meniscus effects at the edges is likely to have increased the local MNW concentrations above the bulk values. Similar, but unidirectional, corrugation has been observed in aligned collagen matrices, but here a bidirectional corrugation is seen which indicates a bi-directional alignment of collagen fibrils thereby warranting further investigation. Therefore, the MNW-collagen matrices were also examined by SEM, Fig. 2. Again, the MNWs did not appear to alter the structure of the collagen except when the matrices contained both MNWs and 0.2 M CDI crosslinking agent.

While SEM is mostly a surface observation, transmittance of polarized light can be used to probe the bulk alignment of a matrix. The transmittance of blank controls and unaligned matrices were fairly flat as a function of angle. However, a four-fold transmission pattern was seen for matrices containing 10million MNW/ml and 0.2 M CDI, Fig. 3. This four-fold symmetry is consistent with the structure suggested by the DIC images in Fig. 1, where the collagen fibrils are oriented in two directions.

The proposed reason for the observed bidirectional alignment is the native structure of the collagen fibril. The spiral structure of the

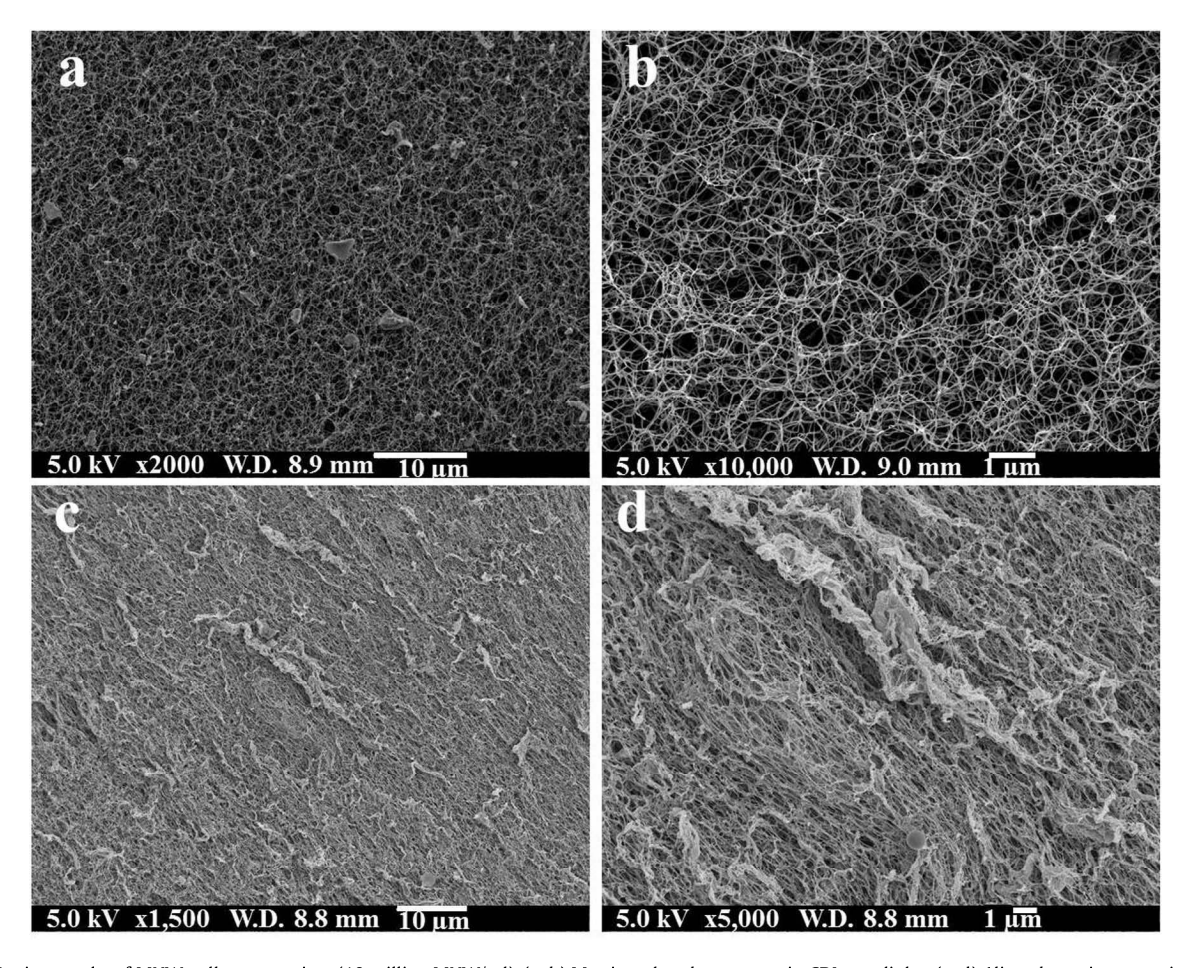


Fig. 2. SEM micrographs of MNW-collagen matrices (10 million MNW/ml). (a, b) Matrices that do not contain CDI crosslinker (c, d) Aligned matrices contained 0.2 M CDI.

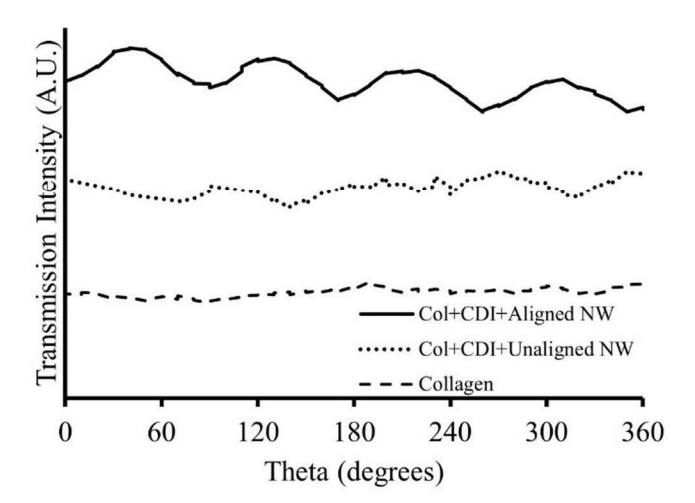


Fig. 3. Transmittance versus angle of polarized light (633 nm) as it passes through collagen matrices. The four-fold nature of transmittance in the first line indicates a matrix containing collagen aligned along two directions. (curves are spaced vertically for observation).

collagen fibril contains a helical angle of $\sim 49^{\circ}-57^{\circ}$ [20,21] as the angle each collagen strand makes with the fibril axis. The observed range of angles from 41° to 54° of the fibrils with respect to the nanowires in the DIC images is similar to reported values of the alphahelical angle associated with type I collagen and suggests that the nanowires potentially covalently bond to the collagen strands.

3.2. Cell studies

Arachnoid cells are sensitive to topographical cues from the extracellular matrix. Here, arachnoid cells were plated on collagen

matrices, incubated until confluence (3 days), and then stained. The blue stain (DAPI) shows the location of the cell nuclei, and the green stain highlights the actin fibers of the cytoskeleton, Fig. 4. Therefore, the green fluorescent signal is an indication of the morphology of each host matrix. The unaligned matrix has a clearly random morphology, whereas the magnetically aligned MNW-collagen matrix has bi-directional alignment that is in agreement with the optical imaging in Fig. 1.

For barcoding cells, it is important to know that the MNWs are adhered to or internalized by cells. Therefore, new MNWs were labeled with RGD, [23] which specifically binds to the integrins that are overexpressed by osteosarcoma cells. After incubation with MNWs, OSCA-8 cells were stained with cell-mask plasma membrane stain (red), lysosensor for lysosomes (green), and Hoechst 33342 nucleic acid stain (blue). The nanowires (black arrows) were internalized by the OSCA-8 cells, as shown in z-sections using 4-channel confocal microscopy as seen at a height (Z) of $-581\,\mu\text{m}$ which corresponded to the center of the cell thickness.

3.3. Barcode readout using first order reversal curves (FORC)

As a proof of concept for using FORC to readout signatures of MNWs, two types of MNWs (Ni with diameter/length = 100 nm/6 μ m & 18 nm/5 μ m) were synthesized and mixed in known amounts for subsequent detection. It has been shown that the MNW diameter is a critical parameter to determine the magnetization reversal mechanism, which in turn determines the MNW coercivity [1,2]. Here, the 100 nm-diameter MNWs are likely to reverse by vortex domain walls, leading to a low coercivity as the magnetic field is swept parallel to the MNW axes. The 18 nm-diameter MNWs on the other hand are likely to reverse via coherent rotation because they are too small to support a vortex core. Therefore, their coercivity is larger at fields parallel to their axes than those

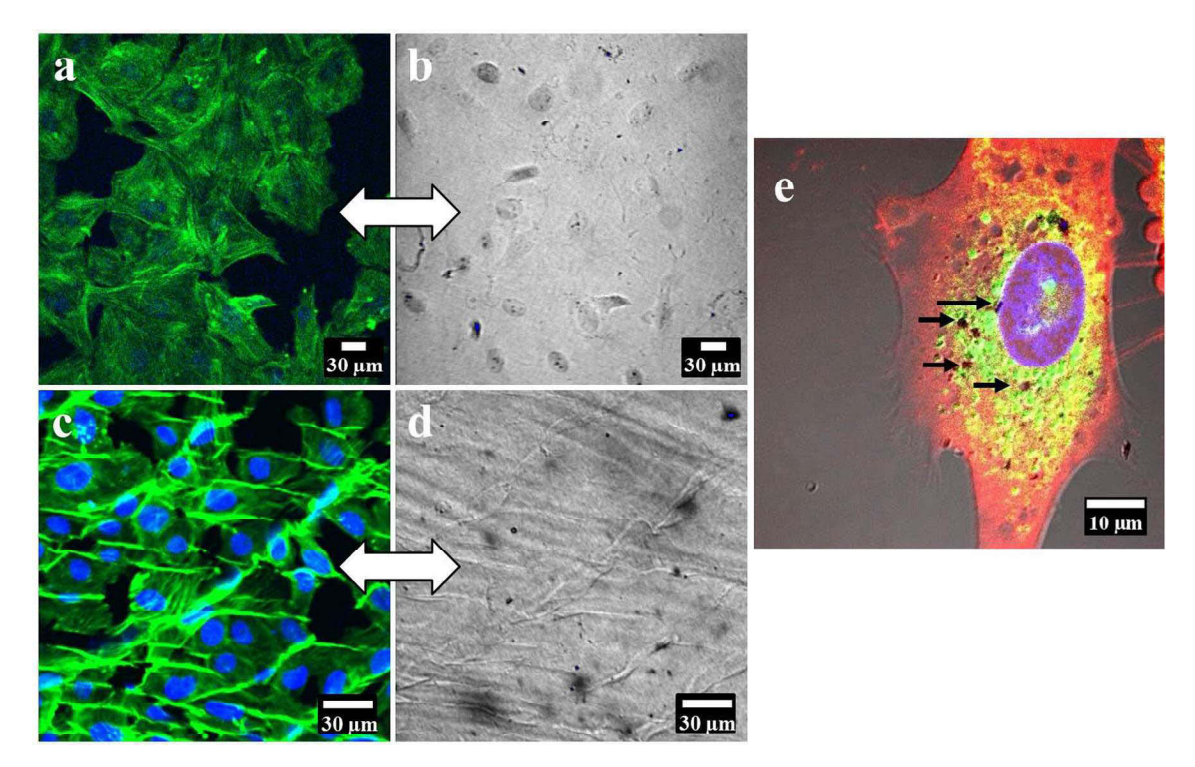


Fig. 4. Contact alignment of arachnoid cells to collagen matrices. (a) Fluorescence and (b) DIC images of unaligned matrix embedded with arachnoid cells stained to show nuclei (blue) and actin (green). (c) Fluorescence and (d) DIC images of magnetically-aligned MNW-collagen matrix (0.2 M CDI, 10million MNW/ml) embedded with stained arachnoid cells. (bars = $30 \mu m$) (e) Z-sections using 4-channel confocal microscopy where the cell membrane is stained red, the lysomes in the center of the cell are stained green and the nucleus is stained blue. The MNWs (black arrows) are observed in the center of the cytosol.

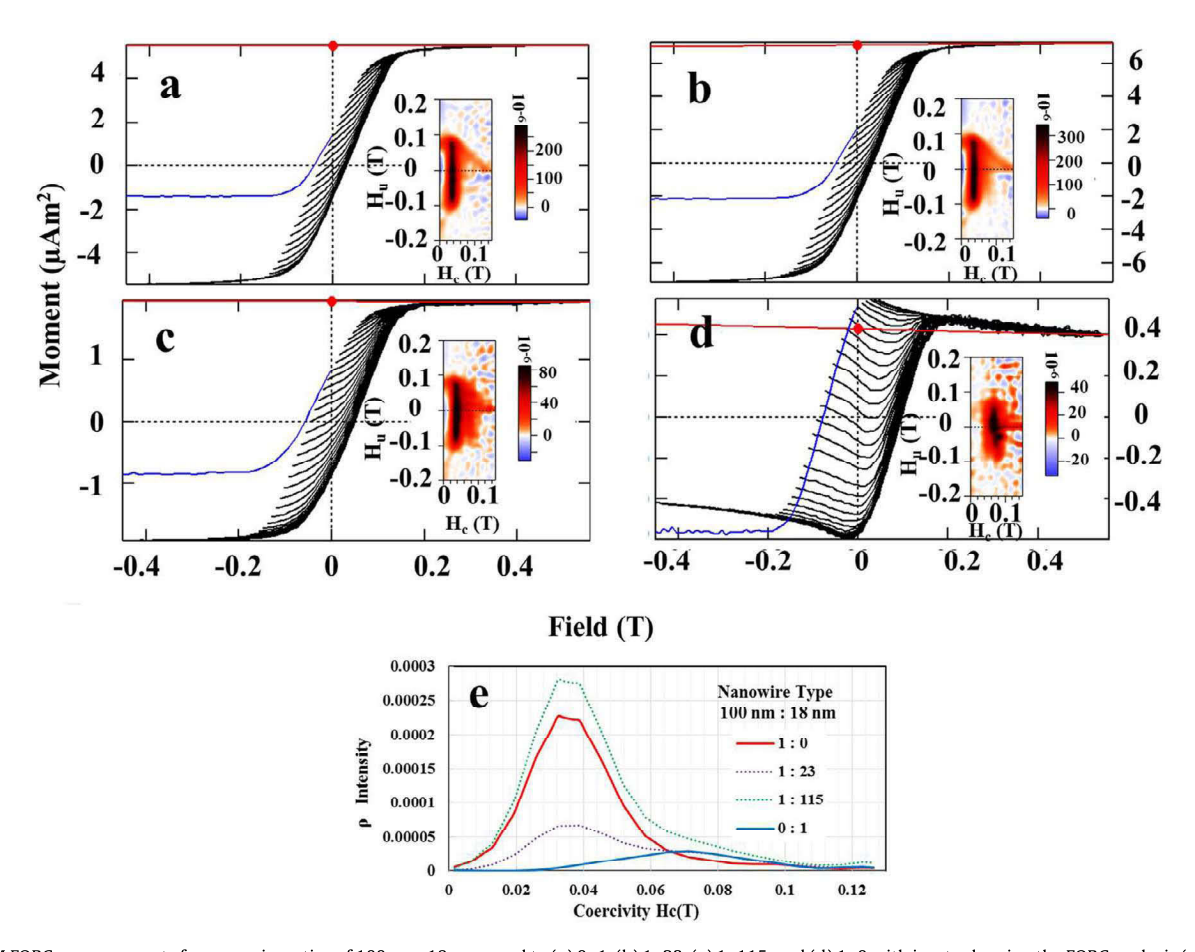


Fig. 5. VSM FORC measurements for nanowire ratios of 100 nm: 18 nm equal to (a) 0: 1, (b) 1: 23, (c) 1: 115, and (d) 1: 0 with insets showing the FORC analysis (ρ vs H_u) using equations 1 and 2. The FORC analysis first corrects for paramagnetic/diamagnetic backgrounds. (e) Integrated intensity of horizontal slices across each FORC analysis diagram.

of the 100 nm-diameter MNWs. A preliminary study (see Supplemental Information) determined the impact of interaction fields between MNWs. Using 100 nm diameter MNWs, long (6 μ m) and short (3 μ m) nanowires that were still in their templates produced high and medium interaction fields between the MNWs, and 6 μ m-long MNWs dispersed in a matrix produced negligible interaction fields on each other. The FORC analysis of coercivity distributions was found to broaden with increasing interaction field, making MNWs more difficult to distinguish. Therefore, large interaction fields were used in this study as a worst-case study of the potential to use FORC for distinguishing MNW barcode signatures.

The FORC data, Fig. 5, is shown as-measured and as-analyzed using the Eqs. (1) and (2). A horizontal slice through the analyzed FORC plots shows the distribution of coercivities as plotted in Fig. 5e. As expected, the 100 nm diameter MNWs had lower coercivities (370 Oe) than the 18 nm diameter MNWs (730 Oe). These end sample curves (100 nm: 18 nm = 1: 0 and 0: 1) were used in a regression analysis to determine the ratio of mixtures which were known to be 100 nm: 18 nm = 23: 1 and 115: 1, respectively. The regressions were both statistically linear and significant, yielding coefficients of $\rho_{100 nm}$: $\rho_{18 nm}$ = 0.75: 1.2 and 0.81: 0.28, respectively.

Before analyzing these ratios, it is important to recall that one type of nanowire ($100 \text{ nm/6}\mu\text{m}$) is larger than the other ($18 \text{ nm/5}\mu\text{m}$). They are both composed of pure Ni, so their volume ratios will equal their mass ratios and the ratios of their moments. Therefore, their volume ratio ($(50/9)^2(6/5) = 37$) can be used to normalize their FORC ratios.

For the first mixture (known ratio of 100 nm: 18 nm = 23: 1), the ratio of the linear regression coefficient, normalized for the volume ratios of the nanowire types, gives the numerical ratio of 100 nm-diameter MNWs per 18 nm-diameter MNW as

$$\begin{split} N_{100\text{nm}}/N_{18\text{nm}} &= (\text{vol}_{100\text{nm}}/\text{vol}_{18\text{nm}}) * (\rho_{100\text{nm}}/\rho_{18\text{nm}}) \\ &= 37 * (0.75/1.2) = 23 \end{split} \tag{3}$$

which is exactly the known value within the error of measurement. For the second mixture (known ratio of 100 nm: 18 nm = 115: 1), the measured ratio of is only 7% less than the known ratio:

$$\begin{split} N_{100\text{nm}}/N_{18\text{nm}} &= (vol_{100\text{nm}}/vol_{18\text{nm}}) * (\rho_{100\text{nm}}/\rho_{18\text{nm}}) \\ &= 37 * (0.81/0.28) = 107 \end{split} \tag{4}$$

4. Conclusions

A surprising bi-directional alignment of collagen fibrils occurred when nickel magnetic nanowires (MNWs) were cross-linked to the collagen and a uniform magnetic field was applied during fixation. This bi-directional alignment was observed by optical DIC microscopy and confirmed by SEM and polarized transmittance. Interestingly, the bi-directional alignment was also confirmed by stained arachnoid cells from the blood-brain-barrier (BBB) as these cells tend to mimic the morphology of their extracellular matrix environment. Hence, this new imaging technique both confirmed the bi-directional alignment, and the resulting matrix also has exciting potential for artificial tissues that mimic

a realistic BBB. It is important to note that the bi-directional alignment was achieved with a single processing step, and did not require layer-by-layer processing. Specific labeling was also achieved for osteosarcoma using RGD-labeled MNWs, leading to the potential to distinguish matrices and cells upon the discovery of an appropriate barcode readout technique. FORC analysis was demonstrated as just such a technique, and it was used to distinguish mixtures of two distinct MNWs at concentrations of 1:23 with negligible error and mixtures of 1:115 with only 7% error. In summary, unique identification of artificial tissues can be achieved by combining the matrix and cell labeling presented here with the magnetic readout technique of FORC.

Acknowledgements

The authors acknowledge support from three UMN sources: Institute of Engineering in Medicine, MN Drive and MN Futures. Parts of this work were carried out in the UMN central facilities: University Imaging Center, Minnesota Nanofabrication Center, and the College of Science and Engineering Characterization Facility, which has received capital equipment funding from the NSF through the UMN MRSEC program under Award Numbers DMR-0819885 and DMR-1420013.

Appendix A. Supplementary data

Supplementary data associated with this article can be found, in the online version, at https://doi.org/10.1016/j.jmmm.2017.11.035.

References

- [1] Sai Madhukar Reddy et al., Electrochemical synthesis of magnetostrictive Fe-Ga/Cu multilayered nanowire arrays with tailored magnetic response, Adv. Funct. Mater. 21 (24) (2011) 4677–4683.
- [2] Sai Madhukar Reddy et al., Magnetization reversal mechanisms in 35-nm diameter Fe1-x Ga x/Cu multilayered nanowires, J. Appl. Phys. 111 (7) (2012), 07A920.
- [3] Liwen Tan, Patrick D. McGary, Bethanie J. H. Stadler, "Controlling the Angular Response of Magnetoresistance in Co/Cu Multilayered Nanowires using Co Crystallographic Orientation,", J. Appl. Phys. 103 (2008) 07B504.
- [4] Wei Hu et al., High-moment antiferromagnetic nanoparticles with tunable magnetic properties, Adv. Mater. 20 (8) (2008) 1479–1483.
- [5] Po-Chiao Lin et al., Ethylene glycol-protected magnetic nanoparticles for a multiplexed immunoassay in human plasma, Small 2 (4) (2006) 485–489.
- [6] Ekaterina I. Galanzha et al., In vivo magnetic enrichment and multiplex photoacoustic detection of circulating tumour cells, Nat. Nanotechnol. 4 (12) (2009) 855–860.

- [7] Hakho Lee et al., Chip-NMR biosensor for detection and molecular analysis of cells, Nat. Med. 14 (8) (2008) 869–874.
- [8] Lu Gao et al., Multiplexing superparamagnetic beads driven by multifrequency ratchets, Lab Chip 11 (24) (2011) 4214–4220.
- [9] Balasubramanian Srinivasan et al., A detection system based on giant magnetoresistive sensors and high-moment magnetic nanoparticles demonstrates zeptomole sensitivity: potential for personalized medicine, Angew. Chem. Int. Ed. 48 (15) (2009) 2764–2767.
- [10] Sebastian J. Osterfeld et al., Multiplex protein assays based on real-time magnetic nanotag sensing, Proc. Nat. Acad. Sci. 105 (52) (2008) 20637–20640.
- [11] A. Curtis, C. Wilkinson, Topographical control of cells, Biomaterials 18 (24) (1997) 1573–1583.
- [12] M.P. Beales, J.L. Funderburgh, J.V. Jester, J.R. Hassell, Proteoglycan synthesis by bovine keratocytes and corneal fibroblasts: maintenance of the keratocyte phenotype in culture, Invest Ophthalmol Vis Sci 40 (8) (1999) 1658–1663.
- [13] T.S. Girton, V.H. Barocas, R.T. Tranquillo, Confined compression of a tissue-equivalent: collagen fibril and cell alignment in response to anisotropic strain, Biomech Eng 124 (5) (2002) 568–575.
- [14] E. Braziulis, M. Diezi, T. Biedermann, L. Pontiggia, M. Schmucki, F. Hartmann-Fritsch, J. Luginbuhl, C. Schiestl, M. Meuli, E. Reichmann, Modified plastic compression of collagen hydrogels provides an ideal matrix for clinically applicable skin substitutes, Tissue Eng Part C Methods 18 (6) (2012) 464–474.
- [15] J.A. Matthews, G.E. Wnek, D.G. Simpson, G.L. Bowlin, Electrospinning of collagen nanofibers, Biomacromolecules 3 (2) (2002) 232–238.
- [16] S. Zhong, W.E. Teo, X. Zhu, R.W. Beuerman, S. Ramakrishna, L.Y. Yung, An aligned nanofibrous collagen scaffold by electrospinning and its effects on in vitro fibroblast culture, J. Biomed. Mater. Res. A 79 (3) (2006) 456–463, https://doi.org/10.1002/jbm.a.30870.
- [17] C. Guo, L.J. Kaufman, Flow and magnetic field induced collagen alignment, Biomaterials 28 (6) (2007) 1105–1114.
- [18] R.T. Tranquillo, T.S. Girton, B.A. Bromberek, T.G. Triebes, D.L. Mooradian, Magnetically orientated tissue-equivalent tubes: application to a circumferentially orientated media-equivalent, Biomaterials 17 (3) (1996) 349–357.
- [19] M.M. Giraud Guille, G. Mosser, C. Helary, D. Eglin, Bone matrix like assemblies of collagen: from liquid crystals to gels and biomimetic materials, Micron 36 (7-8) (2005) 602–608.
- [20] C.H. Lam, E.A. Hansen, A. Hubel, Arachnoid cells on culture plates and collagen scaffolds: phenotype and transport properties, Tissue Eng Part A 17 (13–14) (2011) 1759–1766.
- [21] C. Janson, L. Romanova, E. Hansen, A. Hubel, C. Lam, Immortalization and functional characterization of rat arachnoid cell lines, Neuroscience 177 (2011) 23–34.
- [22] C.H. Lam, E.A. Hansen, C. Janson, A. Bryan, A. Hubel, The characterization of arachnoid cell transport II: paracellular transport and blood-cerebrospinal fluid barrier formation, Neuroscience 222 (2012) 228–238.
- [23] Anirudh Sharma et al., Inducing cells to disperse nickel nanowires via integrinmediated responses, Nanotechnology 26 (13) (2015), 135102.
- [24] Erkki Ruoslahti et al., New perspectives in cell adhesion: RGD and integrins, Science 238 (4826) (1987) 491–498.
- [25] James W. Wells et al., Arginase treatment prevents the recovery of canine lymphoma and osteosarcoma cells resistant to the toxic effects of prolonged arginine deprivation, PloS One 8 (1) (2013) e54464.
- [26] Gerald J. Mizejewski, Role of integrins in cancer: survey of expression patterns, Proc. Soc. Exp. Biol. Med. 222 (2) (1999) 124–138.
- [27] C. Pike, First-order reversal-curve diagrams and reversible magnetization, Phys. Rev. B 68 (10) (2003) 104424.